Polytypism in ZnS, ZnSe, and ZnTe: First-principles study

F. Boutaiba,[1] A. Belabbes,[2,*] M. Ferhat,[1] and F. Bechstedt[3]

[1]*Département de Génie Physique, Laboratoire de Physique des Matériaux et Fluides (LPMF), Université des Sciences et de la Technologie d'Oran, USTO, Oran, Algeria*

[2]*King Abdullah University of Science and Technology (KAUST), Thuwal 23955-6900, Saudi Arabia*

[3]*Institut für Festkörpertheorie und -optik, Friedrich-Schiller-Universität, Max-Wien-Platz 1, 07743 Jena, Germany*

(Received 1 April 2014; revised manuscript received 6 June 2014; published 23 June 2014)

We report results of first-principles calculations based on the projector augmented wave (PAW) method to explore the structural, thermodynamic, and electronic properties of cubic (3C) and hexagonal (6H, 4H, and 2H) polytypes of II-VI compounds: ZnS, ZnSe, and ZnTe. We find that the different bond stacking in II-VI polytypes remarkably influences the resulting physical properties. Furthermore, the degree of hexagonality is found to be useful to understand both the ground-state properties and the electronic structure of these compounds. The resulting lattice parameters, energetic stability, and characteristic band energies are in good agreement with available experimental data. Trends with hexagonality of the polytype are investigated.

DOI: 10.1103/PhysRevB.89.245308 PACS number(s): 71.15.Mb, 71.15.Qe, 71.20.Nr, 61.46.Km

I. INTRODUCTION

Low-dimensional structures such as nanowires (NWs) have received strong interest beginning with the first demonstration in 1991 of synthesizing materials with a least one critical dimension with an extent of only 10–200 nm [1]. Their small diameters, often at distances of only a few times the interatomic distances in crystals, and their unique geometries lead to physical properties which differ drastically from the corresponding bulk material. The chemical and physical properties of NWs can be significantly improved or radically changed as their size is reduced to a nanometer regime, one example concerns the quantum confinement effects. Nanowires are promising structures for applications in future electronic and optoelectronic devices.

In nanowires, the formation of different crystal polytypes is a common phenomenon. Polytypism widely exists in IV-IV, III-V, and II-VI compound semiconductors due to their freedom in the atomic stacking of bilayers consisting of cations and anions. A textbook example is the only stable group-IV SiC compound for which more than 200 polytypes have been observed to date [2]. The most commonly observed polytypes in III-V and II-VI systems are zinc-blende (ZB) and wurtzite (WZ) structures having, respectively, a bilayer stacking of ABCABC in the [111] direction, and ABABAB in the [0001] direction. In fact, theoretical and experimental works have revealed that the ZB (3C) and the WZ (2H) phases are the most common polytypes of III-V and II-VI compounds. The wurtzite and zinc-blende crystal structures share many similarities in terms of atomic arrangements. In both cases, each atom has four nearest-neighbor bonds, and it is only the third-nearest-neighbor geometry that distinguishes the crystal structures with tetrahedrally bonded atoms. The difference in total energies between two phases is small, hence, it gives strong evidence that both of them can be prepared experimentally. Recently, controlled polytypism and twinning in the III-V InAs and InSb nanowires have been realized [3] using metal organic vapor phase epitaxy (MOVPE). X-ray diffraction and transmission electron microscopy were used to an accurate determination of the lattice parameters of ZB, WZ, and 4H polytypes of InAs and InSb NWs. The experimental results show that the occurrence of hexagonal bilayers tend to stretch the distances of atomic layers parallel to the *c* axis and to reduce the in-plane distances compared to those in ZB phase. Moreover, it is found that the lattice parameters scale linearly with the hexagonality of the polytype (i.e., the fraction of bilayers with hexagonal character). Colloidal synthesis of polytypic II-VI nanocrystals with ZB cores and epitaxially grown WZ, such as CdSe [4] and CdTe [5] nanocrystals, are the only few examples of controlled polytype engineering in II-VI systems. Moreover, recent experiments show strong evidence of WZ-ZB polytypism in ZnX (X = S, Se, and Te) materials [6–11]. The twinned ZnX NWs with the mixed ZB/WZ structures are commonly observed along the [111]/[0001] direction.

Although there are many reports of randomly oriented II-VI nanowires that show twinning defects, the various aspects and implications of twinning and polytypism in II-VI compounds are not as well understood as for III-V materials. Indeed, recent *ab initio* studies [12] have addressed the structural, energetic, and elastic properties of cubic (3C) and hexagonal (6H, 4H, 2H) polytypes of III-V compounds GaAs, InP, InAs, and InSb. The obtained structural data enable precise first-principles calculations [13] of the quasiparticle band structure and band alignment of these compounds. In contrast, less is known about the polytypism of II-VI compounds. To the best of our knowledge, there are no theoretical results for polytypism along the row 3C, 6H, 4H, and 2H with increasing hexagonality of the bonding geometry. Yeh *et al.* [14] have addressed the structural properties of 3C and 2H II-VI compounds, and achieved some general relationships between the wurtzite and zinc-blende polytypes for III-V and II-VI compounds. Particularly, it has been concluded that in general the zinc-blende phase is favored as the atomic number of the anion increases (so called anion rule). Only for a few exceptional compounds the anion rule is violated, for instance, for compounds containing first-row cations or the heavy cation Tl and anion Bi. III-nitrides and ZnO tend to adopt the wurtzite structure. Recent first-principles studies [15–17]

*abderrezak.belabbes@uni-jena.de

show that heavier III-V compounds TlSb, TlBi, and InBi stabilize in another polymorph, the tetragonal PbO structure. Yeh *et al.* [18] have addressed the relationship between the band gaps of 3C and 2H III-V and II-VI compounds. Simple rules to predict the basic band structure of wurtzite compounds from its zinc-blende energy levels have been found.

In this paper predictions for the varying physical properties, as lattice constant, local bonding geometry, band gap, etc. are derived versus the stacking sequence of 3C, 2H, 4H, and 6H polytypes in II-VI systems ZnS, ZnSe, and ZnTe. We present extensive first-principles calculations to uncover the structural, energetic, and electronic properties of 3C, 2H, 6H, and 4H polytypes of three II-VI compounds ZnS, ZnSe, and ZnTe using *ab initio* pseudopotential methods and an approximate quasiparticle approach. The paper is organized as follows: In Sec. II we briefly describe the theoretical background of the present work. In Secs. III–V the results are presented and discussed. Finally, conclusions will be given in Sec. VI.

II. COMPUTATIONAL METHODS

Total energy calculations are performed within the density functional theory (DFT) using the local density approximation (LDA) [19] and a plane-wave basis set with the projector-augmented-wave (PAW) method originally developed by Blöchl [20] and adapted by Dal Corso [21] in the Quantum ESPRESSO package [22]. The electron wave functions are expanded within a plane-wave basis set with a kinetic energy of 80 Ry, but an energy cutoff of 600 Ry was included for the charge density. A Gaussian smearing of 0.02 Ry has been applied. The $\boldsymbol{k}$-space integration on the Brillouin zone (BZ) was performed with a $8 \times 8 \times M$ $\boldsymbol{k}$-point mesh

TABLE I. Structural, energetic, and elastic properties of II-VI polytypes. They are computed in the framework of the DFT-LDA method as described in text. The cubic lattice constant a_0 has been recalculated to $a = a_0/\sqrt{2}$ and $c = a_0\sqrt{3}$.

Compound	Polytype		$2c/p$ (Å)	a (Å)	$2c/(pa)$	V_{pair} (Å^3)	ΔE (meV)	B_0 (GPa)
ZnS	2H	Present	6.1349	3.7390	1.6408	37.13	6.5	87.9
		Expt.	6.2610[a]	3.8230[a]	1.6378[a]	39.62[a]		76.2[a]
		Calc.	6.3080[b]	3.8480[b]	1.6392[b]	40.44[b]	8.0[b]	69.7[b]
		Calc.	6.1880[c]	3.7770[c]	1.6380[c]	38.22[c]	6.2[c]	
	4H	Present	6.1227	3.7400	1.6371	37.08	2.33	88.5
	6H	Present	6.1217	3.7410	1.6364	37.09	1.3	84.3
	3C	Present	6.1155	3.7455	1.6330	37.14	0.0	86.3
		Expt.	6.2481[a]	3.8261[a]	1.6330[a]	39.59[a]		76.9[a]
		Calc.	6.2885[b]	3.8509[b]	1.6330[b]	40.38[b]		70.4[b]
		Calc.	6.1718[c]	3.7794[c]	1.6330[c]	38.17[c]		
ZnSe	2H	Present	6.4644	3.9350	1.6428	43.34	9.85	70.9
		Expt.	6.5400[d]	4.0030[d]	1.6337[d]	45.38[d]		80[d]
		Calc.	6.6460[b]	4.0480[b]	1.6417[b]	47.20[b]	9.0[b]	57.1[b]
		Calc.	6.5060[c]	3.9740[c]	1.637[c]	44.49[c]	10.6[c]	
	4H	Present	6.4526	3.9360	1.6394	43.28	4.75	73.7
	6H	Present	6.4445	3.9380	1.6365	43.27	3.0	71.7
	3C	Present	6.4307	3.9380	1.6330	43.18	0.0	71.1
		Expt.	6.5459[a]	4.0085[a]	1.6330[a]	45.52[a]		64.7[e]
		Calc.	6.6210[b]	4.0545[b]	1.6330[b]	47.13[b]		57.3[b]
		Calc.	6.4871[c]	3.9725[c]	1.6330[c]	44.32[c]		
ZnTe	2H	Present	6.9666	4.2330	1.6458	54.05	12.9	54.7
		Expt.	7.0999[f]	4.3200[f]	1.6435[f]	57.37[f]		
		Calc.	7.1780[b]	4.3580[b]	1.6470[b]	59.04[b]	12.0[b]	43.6[b]
		Calc.	6.9890[c]	4.2730[c]	1.6356[c]	55.17[c]	12.8[c]	
	4H	Present	6.9478	4.2370	1.6398	54.00	6.1	57.9
	6H	Present	6.9420	4.2420	1.6365	54.09	3.9	44.2
	3C	Present	6.9337	4.2460	1.6330	54.12	0.0	55.7
		Expt.	7.0309[g]	4.3055[g]	1.6330[g]	56.43[g]		50.9[h]
		Calc.	7.1348[b]	4.3691[b]	1.6330[b]	58.98[b]		43.6[b]
		Calc.	6.9801[c]	4.2744[c]	1.6330[c]	55.22[c]		

[a]Collection of experimental data in Ref. [36].
[b]PAW-GGA from Ref. [37].
[c]LAPW-LDA from Ref. [14].
[d]Collection of experimental data in Ref. [38].
[e]From Ref. [39].
[f]From Ref. [40].
[g]Collection of experimental data in Ref. [41].
[h]Collection of experimental data in Ref. [42].

of Monkhorst-Pack [23]. The value of M has to be varied according to the number of layers in stacking direction of the II-VI polytypes. We use $M = 8, 6, 4$, and 2 for the 3C, 2H, 4H, and 6H polytypes, respectively. The internal atomic positions of 2H, 4H, and 6H polytypes were fully relaxed through minimization of the quantum-mechanical forces on each atom to be below 5 meV/Å. The total energy was converged to within 0.5 meV/cell. The accuracy of the above procedure has been well tested in a previous work [13].

It is known that for semiconductors or insulators, the band gap calculated within the local density approximation or generalized gradient approximation (GGA) underestimates severely the experimental energy gap. To overcome this band-gap problem, we used the recent LDA-1/2 method proposed by Ferreira *et al.* [24,25]. This method meets a precision similar to that of GW approximation [26], which attempts to fix the electron self-energy deficiency of DFT [27].

III. STRUCTURES AND ENERGIES

In order to determine the equilibrium geometries we minimize the total energy E with respect to the atomic coordinates. The independent structural parameters of 2H that need to be determined are V and u, where V is the volume of the unit cell given by a and c are the hexagonal lattice constants, and u is the dimensionless cell-internal parameter, which denotes the position of the second atom along the c axis. The Murnaghan equation of state [28] is applied to determine the equilibrium energy $E = E(V)$ and, thus, the equilibrium volume per II-VI pair $V_{\text{pair}} = \frac{\sqrt{3}}{2}a^2\frac{c}{p}$, the isothermal bulk modulus B_0, and its pressure derivative B_0'.

For ideal, nondeformed bonding tetrahedra it holds $c/a = \sqrt{8/3}$ and $u = 3/8$. A deviation from these values corresponds to a change in the bond angle away from the ideal tetrahedral one. These parameters characterize the atomic geometry and the crystal field by the deviations $[2c/(pa) - 1.633]$ and $[u - 0.375]$. The influence of the optimized u on c/a and V, in general, is very small. However, its small deviation can significantly modify the local electronic properties and internal electric fields due to the spontaneous polarization in hexagonal polytypes [29–33]. This especially holds for heterocrystalline junctions and superlattices [34,35], or the presence of interfaces between two polytypes of one-and-the-same compound in the [0001] direction. In the 4H and 6H polytypes more, three or five, internal-cell parameters have to be optimized. Their influence on the properties is however weaker than that of u in the 2H case.

The results of the structural optimizations for the four polytypes and the three compounds under consideration are given in Table I. The polytypes are ordered according to their hexagonality, defined by the ratio of the number of the hexagonal bilayers to the total number of bilayers per unit cell (cf. Fig. 1). Between the most extreme polytypes 3C with $h = 0\%$ and 2H with $h = 100\%$, one finds the intermediate polytypes 6H with $h = 33\%$ and 4H with $h = 50\%$. For 2H we find good agreement between the calculated and the experimental lattice constant a, apart from the rather weak underestimation of a, a well know feature of the LDA. However, the ratio c/a of the wurtzite structure 2H agrees

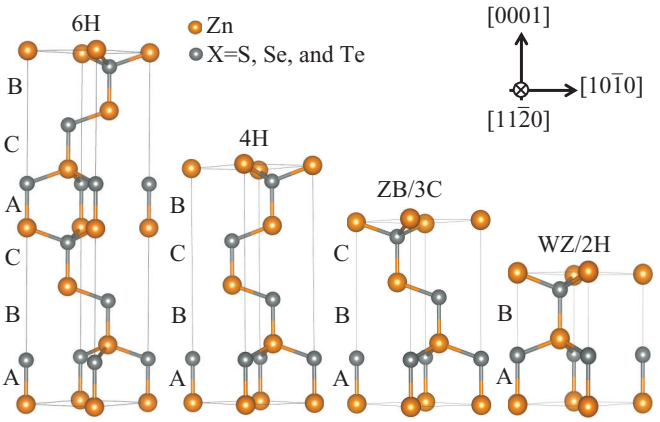

FIG. 1. (Color online) Stick-and-ball models of 3C and pH (p = 2, 4, 6) of ZnX polytypes. Zinc: brown spheres, X (X = S, Se, and Te): gray spheres. The stacking sequence of the cation-anion bilayers are indicated by the symbols A, B, or C. Primitive unit cells are shown for the pH polytypes, while a nonprimitive hexagonal cell is depicted to illustrate the 3C symmetry.

perfectly with experiment. The deviations do not exceed 1% (see Table I). The error introduced by the LDA due to the overbinding effect is expected to be very similar for the other hexagonal polytypes 4H and 6H. The underestimation of the lattice constants by less than 1% does not play a role since we consider only the relative variations of Δa and Δc using ZB values as reference in Table II.

In Fig. 2(a) the lattice constant ratio $2c/(pa)$ is plotted versus the percentage of hexagonality h of the polytype. For the three II-VI compounds the cell shape increase monotonously with h along the row 2H, 4H, 6H, and 3C. The variation with the anion X = S, Se, and Te as a function of hexagonality reflects the chemical trend with respect the anion size and the average of the bond ionicities 0.673 (0.677) ZnS/0.597(0.639) ZnSe/ZnTe(0.684) [43] ([44]). The same holds for the deviation of u from its ideal value $u = 0.375$, in the wurtzite (2H) case with $u = 0.3745$, 0.3744, and 0.3742 for ZnS, ZnSe, and ZnTe, respectively.

These findings are in agreement with other predictions for the ZB-WZ polytypism in semiconductors. Only slightly larger values of $u = 0.375$ for ZnX compounds have been found by

TABLE II. Relative deviations (with inclusion of the finite cell-internal parameters) of lattice constants from those of the most stable 3C polytype (in percent) from Table I.

Compound	Polytype	$\Delta c/c$	$\Delta a/a$	$\Delta\frac{2c}{pa}/\frac{2c}{pa}$
ZnS	2H	0.32	0.16	0.48
	4H	0.12	0.13	0.25
	6H	0.10	0.10	0.21
ZnSe	2H	0.52	0.07	0.60
	4H	0.34	0.05	0.39
	6H	0.21	0.00	0.21
ZnTe	2H	0.47	0.30	0.78
	4H	0.20	0.21	0.41
	6H	0.12	0.09	0.21

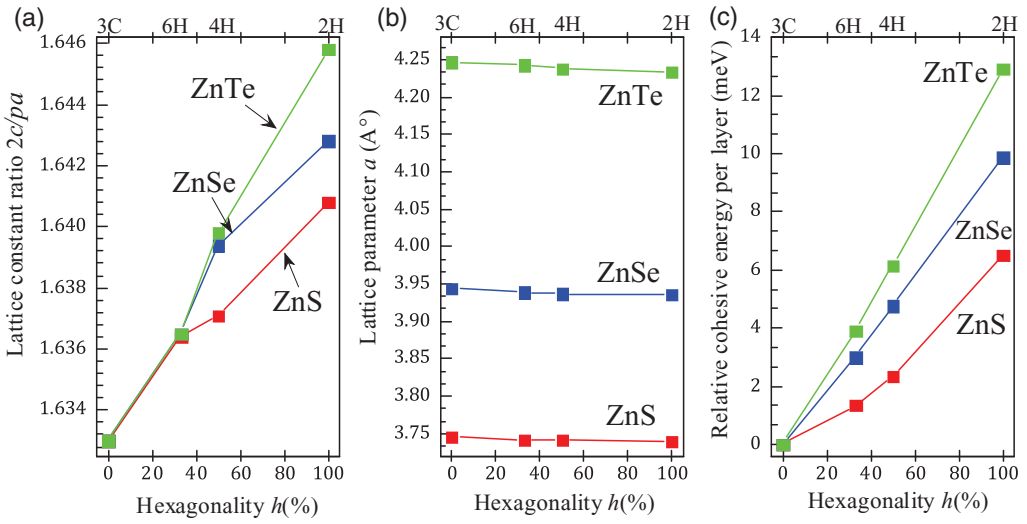

FIG. 2. (Color online) Structural and energetic properties as function of the hexagonality of the polytype. (a) Renormalized lattice constant ratio $2c/(pa)$. (b) Lattice parameter a. (c) Cohesive energy per cation-anion pair relative to the 3C value. Lines are only given to guide the eye.

Yeh *et al.* [14]. Biering *et al.* [37] predicted values 0.3747 for ZnS, 0.3743 for ZnSe, and 0.3733 for ZnTe. For ZnS, Kisi *et al.* [45] using powder neutron diffraction analysis obtained a value of 0.3747, in good agreement with the calculated values. The fact that $u < 0.375$ can be explained by a balance of repulsive and attractive electrostatic interactions of bonds depending on their stacking, length, and ionic degree [46].

The behavior found for $2c/pa$ versus hexagonality h for all ZnX (X = S, Se, and Te) compounds in Fig. 2(a) corresponds to an increasing deformation of the bonding tetrahedra, which are stretched along the c axis and, hence, a certain biaxial strain in the hexagonal polytypes compared to 3C. We also observe a strong deviation of the cell-shape parameter $2c/pa$ from its linear variation from 3C to 2H, as a function of the number of bond inversions along the stacking direction, indicating a stronger distortion of the bonding tetrahedra. The distortion in the close-packed plane due to the hexagonality change is much higher than for III-V compounds and SiC [47,48]. This fact is clearly visible in Fig. 2(a). The deviation is obviously a consequence of cell-internal relaxation which gives additional degrees of freedom and hence a higher flexibility of the bonds, leading to larger relative changes of $\Delta a/a$ and $\Delta c/c$ with respect to the zinc-blende values (see Table II). These deviations from bulk ZB bond length can be explained due to the changed stacking sequence of the bilayers and concomitantly changed the third next-nearest-neighbor distance. We note that atomic relaxations for all II-VI compounds are not very large. Nevertheless, they are very important for stabilization of hexagonal polytypes. The influence of the modified bond stacking is significant for the 2H and 4H polytypes, and the maximum deviation occurs for ZnTe.

In addition, we find that the lateral lattice parameter a nearly linearly decreases with rising hexagonality (h) [see Fig. 2(b)]. This happens for all considered II-VI compounds. A best fit to the calculated lattice parameters of ZnS and ZnSe gives, respectively, $a(h) = 3.745 - 0.013h + 0.007h^2$ and $a(h) = 3.944 - 0.02h + 0.01h^2$ leading to a weak lattice parameter bowing of $b(a) = 0.007$ Å for ZnS, and $b(a) =$ 0.01 Å for ZnSe. This weak variation indicates that the lattice parameters a for these compounds are insensitive to the hexagonality, similar to the case of III-V polytypes (see Ref. [46] and references therein). Note that the volume is almost conserved and does not show a clear trend with respect to the hexagonality, we note also that the averaged elastic properties represented by the bulk modulus vary only weakly with the polytype.

There is a clear correlation between the geometrical effect and the cohesive energy of the polytypes, as indicated in Fig. 2(c). In all cases, the zinc-blende structure 3C is slightly more stable than the wurtzite one 2H as experimentally observed [49,50], but the energy difference is so small that it might be taken as an indication of the occurring polytypism. The calculated total energy differences per pair between 2H (WZ) and 3C (ZB) are 6.5, 9.8, and 12.9 meV for ZnS, ZnSe, and ZnTe, respectively. They are comparable with those calculated by Yeh *et al.* [14] of 6.2 meV for ZnS, 10.6 meV for ZnSe, and 12.8 meV for ZnTe. The total energy per pair of a polytype relative to the 3C structure as function of hexagonality [see Fig. 2(c) and Table I] follows a clear chemical trend. The variation of the total energy shows a relative strong linearity versus hexagonality for ZnSe and ZnTe, while a nearly parabolic dependence on the hexagonality is observed for ZnS. The calculated cohesive energy is ordered according to $E_{2H} < E_{4H} < E_{6H} < E_{3C}$. The 3C polytype is the stable, followed by 6H, 4H, and 2H polytypes. Compared to the large absolute values of the cohesive energies of the II-VI compounds, the small variations in Fig. 2(c) indicate that it costs an extremely low energy to change the sequence of the stacking layers. In fact, the calculated total energies for the polytypes are so close that their stability may be significantly affected by the temperature and crystal growing conditions, confirming the polytypism observed in these compounds. This explains why ZnS can be grown not only in ZB but also in WZ structure [10,51].

Most important, however, are the small energy differences between 3C and 6H polytypes. One clearly observes a tendency for the stronger energetical favorization of bond twisting in these compounds. Our calculated total energies for the 6H

ZnS, ZnSe, and ZnTe structures relative to 3C structure are 1.3, 3.0, and 3.9 meV, respectively, which may indicate good chances for the preparation of 6H polytypes, e.g., in nanorods. From a thermodynamic point of view, the tendency of the formation of hexagonal structures should be more pronounced in ZnS in comparison to ZnTe and ZnSe, as can be also seen in Fig. 2(c).

IV. STACKING-FAULT FORMATION

The four polytypes differ only in the stacking sequence of the tetrahedra along the [0001] direction. The resulting one-dimensional character of the stacking suggests the description of the polytypes in a one-dimensional Ising-type model, the ANNNI (axial next-nearest-neighbor Ising) model [53]. In this model, each bilayer i is characterized by a spin variable $\sigma_i = \pm 1$ according to the orientation of the bonding tetrahedra. The total energy of the system can be described by parameters J_j as the interaction energies of two bilayers. The three interaction parameters J_1, J_2, and J_3 are deduced from the relative total energies of ΔE(2H), ΔE(4H), and ΔE(6H) with respect to the 3C phase [46,53]. This has been widely demonstrated for IV-IV materials [47,48,54–57], but also for III-V compounds [46,58]. The resulting values J_1, J_2, and J_3 are listed in Table III.

There are clear trends for the interaction parameter values. We observe a tendency for a reduction of J_1, J_2, and J_3 with the anion along the row Te, Se, and S. The nearest-neighbor bilayer interaction leads to the dominating positive parameter J_1, while the second and third nearest-neighbor interactions J_2, and J_3 are much smaller and possess the negative sign. We note that the interaction between the nearest-neighbor layers is at least 7 times larger in magnitude than between second-neighbor layers. This dominance is similar to results obtained earlier for GaP [46].

In Table III the parameters J_1, J_2, J_3 and their ratios show that ZnS is closer to the phase boundary 3C-6H and rather near the multiphase degeneracy in a phase diagram versus J_1/J_2 and J_3/J_2 [46]. Therefore, ZnS should show the strongest stacking fluctuations in the nanorods under equilibrium conditions, and hence the strongest tendency to grow within a hexagonal polytype, at least in a nanowire. The occurrence of wurtzite has been confirmed by experiments [10,51,59]. The coexistence of wurtzite and zinc-blende regions and their intermixing through stacking faults on the (111) planes have also been pointed out by Heine *et al.* [60] for bulk systems.

It is instructive to compare the interaction parameters J_1, J_2, and J_3 for II-VI compounds with those of III-V systems [12,46]. The overall agreement concerning the sign and magnitude of the interaction parameters compared to III-V compounds without the first-row anion N is quite reasonable. In the case of GaAs, the sign of the J_i are the same of those of the ZnX compounds, but J_1 is larger compared to II-VI compounds. This fact is obviously due to higher ionicity in the II-VI compounds compared to the GaAs. In contrast AlN crystalizes within the wurtzite structure under ambient conditions. Its stabilization is, however, due to the preference for opposite ANNNI spins in adjacent bilayers. This behavior stabilizes a hexagonal phase. The preferred zinc-blende compared to wurtzite structure of conventional II-VI and III-V compounds is clearly correlated with the sign of J_1, which can be explained by the electrostatic contribution and the electronegativity difference between AB compounds. Their balance can drive the value of J_1 from positive to negative and hence change the stable structure from the zinc blende to wurtzite. In the case of AlN, the J_1 is drastically reduced and have opposite sign, whereas the second and third nearest-neighbor interaction energies J_2 and J_3 are negative and much larger.

Besides the polytypism, the ANNNI model also enables one to discuss some two-dimensional defects in cubic crystals, like the stacking faults. The most common stacking faults are the intrinsic stacking fault (ISF) and the extrinsic stacking fault (ESF) [56,61–63]. The ISF and ESF are related to the bond tetrahedron rotation in two bilayers and differ by the distance of the two perturbed bilayers by one or two bilayers. The ISF can be thought of as removing one bilayer from the infinite 3C stacking sequence. Instead, the ESF can be thought of as adding one bilayer to the stacking sequence, for example, due to condensation of eigeninterstitials. Adding a C bilayer, the resulting stacking sequence is ABCA/C/BCABC. . . . The occurrence of such stacking faults can be also discussed in terms of a twist by 180° of the three equivalent bonds between two bilayers in a bonding tetrahedron which are not parallel to the [111] axis. Then, besides staggered (cubic) layers, also eclipsed (hexagonal) bilayers appear [63].

The formation energy E(ISF/ESF) of a stacking fault per two-dimensional unit cell perpendicular to the stacking direction is given within the ANNNI model by [56,63]

$$\Delta E_{\mathrm{ISF}} = 4J_1 + 4J_2 + 4J_3, \quad \Delta E_{\mathrm{ESF}} = 4J_1 + 8J_2 + 8J_3. \tag{1}$$

The stacking fault energies γ(ISF/ESF) per unit area follow from the values of Eq. (1) by division with the area $\sqrt{3}a_0^2/4$ of one atom in a (111) plane. Such values are listed in Table III together with results of measurements [52]. The calculated values show a clear chemical trend of the formation energies of ISF and ESF with respect to the anion size, a

TABLE III. Parameters of the ANNNI model (in meV per pair) and resulting stacking fault formation energies ΔE_f (meV/atom) and γ (mJ/m^2) for the 3C polytype. The experimental values are taken from Ref. [52].

						ESF		ISF		SF	
Compound	J_1	J_2	J_3	J_3/J_2	J_1/J_2	ΔE_f Calc.	γ Calc.	ΔE_f Calc.	γ Calc.	ΔE_f Expt.	γ Expt.
ZnS	3.41	−0.46	−0.16	0.34	−7.41	28.53	21.64	14.71	11.16	$\leqslant 6$	$\leqslant 5$
ZnSe	5.06	−0.09	−0.13	1.44	−56.22	33.68	28.24	23.08	19.36	13 ± 1	11 ± 1
ZnTe	6.59	−0.15	−0.14	0.93	−43.93	35.24	34.36	25.84	25.2	16 ± 2	16 ± 2

significant increase with rising size of the anion. This trend is consistent with the wurtzite/zinc-blende energy differences for these compounds. The estimated fault energies are all positive (see Table III), which is in agreement that hexagonal polytypes of these materials are not observed under ambient conditions. Those in ZnS have the lowest formation energy, followed by ZnSe and then ZnTe. Note that the ISF is the most favorable defect. The stacking fault energies in Table III are much smaller than those for conventional III-V compounds such as GaAs [46]. Again, this is a hint that this should be a good chance to grow hexagonal polytypes of ZnX compounds. From the energetic point of view, it is much easier to generate stacking faults in ZnS crystals than in ZnSe and ZnTe. This is possibly one part of the explanation for the large variety of hexagonal polytypes like 8H and 10H which appeared along the entire wire length in turns [51]. In addition, the energy results help to explain the difficulty in growing wurtzite films, particularly for ZnSe and ZnTe. The small energy difference between cubic and wurtzite structures in ZnS makes it energetically favorable to introduce stacking faults in zinc-blende films, thereby switching to the wurtzite structure.

Experimentally it is rather difficult to distinguish between extrinsic and intrinsic stacking faults in zinc-blende crystals. In the literature [52] only formation energies of stacking faults (SFs) are listed. Nevertheless, the low formation energy of the intrinsic stacking fault is consistent with experimental observations by Takeuchi *et al.* [52], who estimated the formation energy based on the width of 60° dislocations. They found the same energetic ordering of the faults as that in Table III. However, their formation energies are consistently smaller than the computed ones. We should mention that the agreement between the calculated stacking fault energies with the experimental values is quite good taking into consideration the complicated procedures to extract such energies from experimental data.

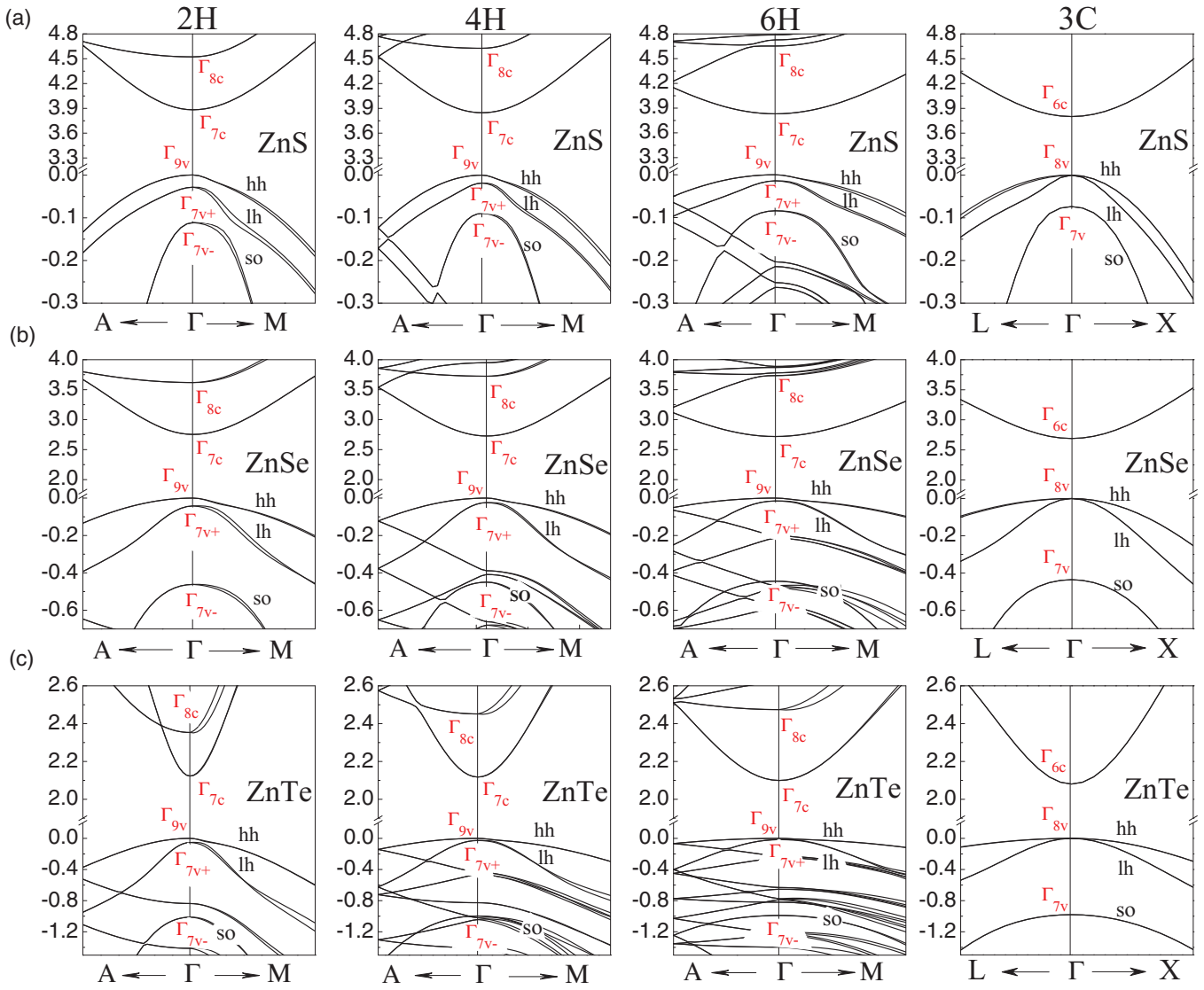

FIG. 3. (Color online) The uppermost valence and lowest conduction bands near Γ of the hexagonal polytypes and 3C of (a) ZnS, (b) ZnSe, and (c) ZnTe. The valence band maximum is used as energy zero. The symmetry of the most important states is indicated.

V. QUASIPARTICLE BAND STRUCTURES

We apply the LDA-1/2 method [24,25] by preparing a pd-like excitation in the electronic system of ZnX (X = S, Se, and Te) for which the exchange-correlation XC is treated by the LDA functional [73]. This approach allows the inclusion of spin-orbit interaction in a rather easy manner, which usually works very well and gives very good results for the band gaps, bandwidths, and band dispersions [74–81]. In addition, it compares well with results of the GW quasiparticle (QP) approach [26,72,82–84].

The QP self-energy effects are simulated by a hole excitation whose extent is derived by maximizing the fundamental energy gap of 3C. The extent is characterized by a characteristic radius CUT. For ZnX the excitation possesses 50% p and 50% d character, in which the variation of the character yields to similar gaps as predicted in the original paper [24]. Consequently, the eigenvalues with p or d character are corrected, mainly shifted to lower or higher energies according to their occupation. In principle we follow the line to introduce empirical corrections to the potentials of the DFT-LDA in order to account for the excitation aspect. In contrast to a scissors operator, the corrections within the LDA-1/2 method also can modify the band dispersion and can give reasonable values for interband energies at different high-symmetry points in the BZ. We note that the LDA-1/2 method is devised for the calculation of excited states and not for ground state. The group II-VI compounds are characterized by a relatively small energy difference between the d electrons of the semicore shell and the anion p and cation s electrons of the valence shell. Therefore, the influence of the semicore d states on the valence- and conduction-band structures is very strong in compounds of these elements. The corrections of both Zn d state and X = S, Se, and Te p states are more important for the valence-band width and energy-gap value. From a computational point of view, the calculation of a LDA-1/2 electronic structure is as fast as a conventional LDA calculation and hence demands much less computer resources than the HSE + G_0W_0 method [85]. This holds especially for the 6H polytype whose unit cell contains 12 atoms (see Fig. 1). The quasiparticle (QP) band structures for 2H, 4H, 6H, and 3C polytypes of ZnS, ZnSe, and ZnTe are computed within the LDA-1/2 method including spin-orbit interaction around the fundamental gap that are displayed in Fig. 3. The various band parameters values, as band gap (E_g), spin-orbit splitting energy (Δ_{so}), and crystal field splitting (Δ_{cf}) compared to experimental and theoretical values are given in Table IV.

The two QP band structures in Fig. 3 for 2H and 3C show several similarities. All band structures show a pronounced minimum of the lowest conduction band (CBM) at Γ point in the BZ center. The energy positions of the S, Se, Te s state and the widths of mainly anion-derived valence bands turn out to be similar for both polytypes. Only the number of bands is doubled in agreement with the small BZ in the 2H case. The similarities are understandable in terms of the fact the tetrahedral nearest-neighbor configurations are similar in both cases. The principal features of the band structures of the hexagonal pH polytypes can be partially understood by folding arguments. In the case of wurtzite the levels are doubled at Γ (with respect to the zinc-blende structure) due to the band folding along the [111]/[0001] direction. In particular, this holds for the bands along the high-symmetry Γ-A line, which are clearly a result of the folding of the bands along the Γ-L line in the fcc BZ onto the Γ-A line in the hexagonal BZ. For instance, one L point in the fcc BZ is folded onto the Γ point of the 2H BZ. Such a folding procedure has also consequences for the interpretation of the polytype bands. For instance, to

TABLE IV. Characteristic parameters of the band structures from LDA-1/2 QP calculations including spin-orbit interaction for four polytypes of three II-VI compounds. Band gap energies E_g (eV), spin-orbit splitting energy Δ_{so} (in meV), and crystal-field splitting Δ_{cf} (in meV). The results are compared with values from other calculations and experiment.

	Polytype		E_g (eV)	Δ_{so} (meV)	Δ_{cf} (meV)
ZnS	2H	Present	3.88	80.95	59.35
		Calc. (HSE + G_0W_0)	4.08[a]		
		Calc. (GW)	3.98[j]		
		Expt.	3.86[b]	92[c]	58.00[c]
		Expt.	3.91[d]		
	4H	Present	3.84	74.65	33.45
	6H	Present	3.83	74.13	24.16
	3C	Present	3.80	73.6	0.00
		Calc. (GW)	3.98[j]		
		Calc. ($G'W'$)	3.80[k]		
		Expt.	3.82[e]	86[f]	
ZnSe	2H	Present	2.75	437.2	66.7
		Calc. (HSE + G_0W_0)	2.99[a]		
		Calc. (GW)	2.84[j]		
		Expt.	2.87[a]		
		Expt.	2.71[d]		
	4H	Present	2.72	436.36	37.23
	6H	Present	2.71	436.13	23.37
	3C	Present	2.69	435.6	0.00
		Calc. (GW)	2.84[j]		
		Calc. ($G'W'\Gamma$)	2.68[k]		
		Expt.	2.70[g]	420[f]	
ZnTe	2H	Present	2.12	983.59	81.35
		Calc. (HSE + G_0W_0)	2.58[a]		
		Calc. (GW)	2.57[j]		
		Expt.	2.39[d]		
	4H	Present	2.12	983.42	42.28
	6H	Present	2.10	981.70	24.72
	3C	Present	2.09	980.10	0.00
		Calc. (GW)	2.57[j]		
		Calc. ($G'W'\Gamma$)	2.27[k]		
		Expt.	2.26[h]	950[i]	

[a]Reference [64].
[b]Reference [49].
[c]Reference [36].
[d]Reference [65].
[e]Reference [66].
[f]Reference [67].
[g]Reference [68].
[h]Reference [69].
[i]Reference [70].
[j]Reference [71].
[k]Reference [72].

understand the lowest conduction bands one has to fold the L_{6c} zinc-blende state onto the Γ point, giving rise to the Γ_{8c} state in wurtzite crystals. It is usually above the pure s-like state Γ_{7c}, which arises from the Γ_{6c} level in the zinc-blende case. However, due to the slightly changed bonding behavior in the hexagonal 2H crystal, the energetical order of the two levels Γ_{1c} and Γ_{3c} without spin-orbit interaction (Γ_{7c} and Γ_{8c} with spin-orbit interaction) depends sensitively on the atomic geometry and the strain state. In any case for all hexagonal ZnX polytypes the Γ_{8c} level is above the Γ_{7c} level. This ordering is important because only optical transitions from the Γ_{9v} and Γ_{7v} valence states into the Γ_{7c} conduction band states are essentially dipole allowed.

As a consequence of the LDA-1/2 approach, the Zn-derived semicore d states shift down by about 1 eV relative to the LDA positions (not shown here). This happens for all considered II-VI compounds. The d electron bands are located at -7.41, -7.99, and -8.62 eV for ZnS, ZnSe, and ZnTe. The resulting d position for ZnX with respect to the VBM is close to those predicted from photoemission measurements [42]. Those results are in excellent agreement with the theoretical study at the G_0W_0 level by Fleszar and Hanke [72], who predicted similar values of -7.49 for ZnS, -7.82 for ZnSe, and -8.43 for ZnTe. For ZnS, Shishkin and Kresse [84] obtained a value of -7.5 eV, also in good agreement with the present value. Furthermore, we observe that the calculated band gap for a hexagonal polytype is larger than that of the zinc-blende crystal. Very recent calculations using the more sophisticated HSE + GW method [85] by Yadav and Ramprasad [64] also confirm that the band gap increases from 3C to 2H (see Table IV).

Our calculated band gaps for 3C (2H) ZnX polytypes are in excellent agreement with experiment. The calculated values of 3.80 (3.882) eV, 2.69 (2.753) eV, and 2.127(2.090) eV compare well to the measured values of 3.82 (3.860) eV, 2.70 (2.874) eV, and 2.26 (2.39) eV for ZnS, ZnSe, and ZnTe, respectively. The mean absolute relative error of the computed gaps amounts to 2.5% and, hence, indicates a high predictive power of the LDA-1/2 method for the band structures of the polytypes around their fundamental gaps.

There is a clear chemical trend for the band gap values with respect to the semicore d states versus the anion size for hexagonal and cubic structures. This reduction is due to the fact that the p-d interaction shifts the anionic p bands closer to the Zn s conduction bands. Since the binding energy of the semicore d states increases from ZnS to ZnTe the p-d interaction decreases along the row, and the gap shrinkage decreases accordingly. This is important information concerning not only II-VI compounds, but valid for all cases where localized d orbitals must be treated explicitly [72,84,86–88]. Our results demonstrate that the LDA-1/2 approach yields excited electronic properties for compounds such as II-VI and other materials [24,25] with a precision close to that taking the true GW XC self-energy into account. This holds especially for the energy range around the fundamental gap (see Table IV) and hence suggests a similar accuracy also for other hexagonal polytypes in this energy range.

From the band structures in Fig. 3, we derive the most important splitting parameters of the valence bands. Within the quasicubic approximation (where the anisotropy of the spin-orbit interaction in the pH polytypes is neglected) only the spin-orbit splitting Δ_{so} of the pure p states and the crystal-field splitting Δ_{cf} (characterizing the hexagonal crystal field) are relevant.

At first glance, the uppermost valence bands at Γ of the hexagonal crystals are similar to that of 3C. Only the (positive) crystal-field splitting Δ_{cf} (see Fig. 3) leads to an additional splitting of the Γ_{8v} state in 3C besides the Γ_{8v}-Γ_{7v} splitting due to the spin-orbit interaction. In wurtzite crystals, one expects a sequence of the valence levels Γ_{9v}, Γ_{7v+}, and Γ_{7v-}, which is present in Fig. 3. In the 4H and 6H structures, more folded bands come in because of the increase in the period of the superlattices along the hexagonal axis. For ZnSe and ZnTe, a problem arises due to the two (with spin four) relatively flat valence bands along the ΓL line in 3C. As shown in Figs. 3(b) and 3(c), the uppermost twofold (with spin) degenerate levels

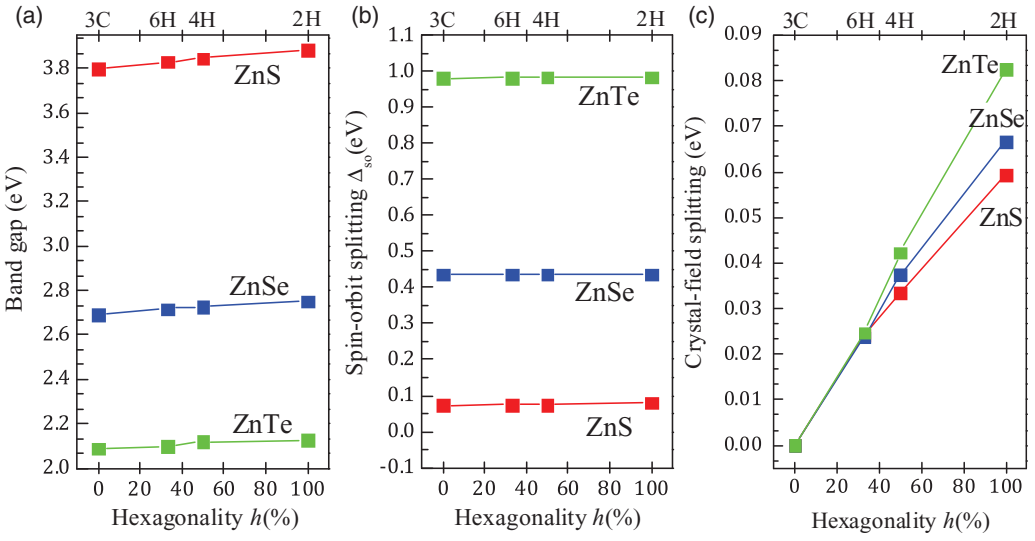

FIG. 4. (Color online) Band gap (a), spin-orbit splitting (b), and crystal-field splitting (c) vs polytype hexagonality h.

TABLE V. Effective electron and hole masses (in units of free-electron mass m_0) near to Γ of zinc-blende (3C) II-VI compounds for different orientations as obtained in LDA-1/2. The results are compared with values from other calculations and experiments.

Compound	Method	m_e	m_{hh}^{100}	m_{hh}^{111}	m_{lh}^{100}	m_{lh}^{111}	m_{so}^{100}	m_{so}^{111}
ZnS	LDA-1/2	0.302	1.051	1.640	0.230	0.208	0.601	0.590
	LDA+U[a]	0.176	1.023	1.687	0.268	0.218	0.512	0.447
	LDA[a]	0.150	0.775	2.755	0.224	0.188	0.385	0.365
	Expt.[b]	0.340		1.760				
ZnSe	LDA-1/2	0.154	0.634	1.967	0.206	0.129	0.308	0.306
	LDA+U[a]	0.100	0.636	1.920	0.129	0.117	0.287	0.309
	LDA[a]	0.077	0.564	1.924	0.104	0.094	0.250	0.254
	Expt.[b]	0.170	0.570					
ZnTe	LDA-1/2	0.115	0.490	0.774	0.166	0.110	0.290	0.291
	LDA+U[a]	0.081	0.483	1.318	0.096	0.085	0.288	0.290
	LDA[a]	0.064	0.381	1.119	0.071	0.066	0.254	0.256
	Expt.[b]	0.130						

[a]From Ref. [90].
[b]From Ref. [91].

Γ_{9v} and Γ_{7v+} can still be clearly identified. However, while in the 2H case the $L_{4,5v}$ and L_{6v} levels are folded onto Γ states below Γ_{7v-} (at least for ZnSe), the valence band states from 1/2 ΓL (4H) or 1/3 ΓL and 2/3 ΓL (6H) are folded onto energies at the Γ point near to the Γ_{7v-} level (4H) or even above it for both ZnSe and ZnTe. Therefore, we did a careful symmetry analysis of the valence states at Γ to identify the Γ_{7v-} band which mainly consists of atomic p_z-like orbitals. For instance, the figure panels for ZnTe show that the fifth (seventh) twofold degenerate level below VBM corresponds to Γ_{7v-} in the 4H (6H) case.

For all compounds, the crystal-field splitting Δ_{cf} increases monotonously with the polytype hexagonality h and the anion size [see Fig. 4(c) and Table IV]. The increase is almost linear. The 2H structure has the largest band splitting reflecting the highest hexagonal crystal field, which is in agreement with the increase of the aspect ratio c/a and the deviation of u from its ideal value $[u - 0.375]$. Our calculated value of 59.4 meV for 2H ZnS agrees very well with the measured value of 58 meV. However, no values are available for other II-VI polytypes.

Concerning the spin-orbit splitting Δ_{so}, the variation is completely different. The chemical trends with the anion along S, Se, and Te are unique, they increase with the anion size going from ZnS to ZnTe. However, the position of the Γ_{7v-} level is independent of the polytype, and is rather constant with respect to the VBM (Γ_{9v}) [see Figs. 3 and 4(b)]. As a long-range interaction the hexagonal crystal field hardly influences the spin-orbit coupling constant for the valence p electron states. Our calculated Δ_{so} for 3C ZnX and 2H ZnS are in excellent agreement with experimental data. However, no experimental values are available for 4H and 6H polytypes of ZnS, and 2H, 4H, and 6H polytypes of ZnSe and ZnTe.

The variation of the band gap E_g versus hexagonality h is given in Fig. 4(a) and Table IV. There are clear chemical trends for band gap energy with respect to the anion size and hexagonality h. The band structures of the ZnX polytypes indicate that the conduction band minima occur at the Γ point rendering all polytypes direct semiconductors. We note that E_g increases weakly from a 3C ($h = 0\%$) to 2H ($h = 100\%$) structure. A fit with a concave curve gives a weak negative band gap bowing of $b = -0.016$, -0.026, and -0.05 eV for ZnS, ZnSe, and ZnTe, respectively. We observe a clear trend of the absolute variations of the gaps going from 3C to 2H: 82 (ZnS), 60 (ZnSe), and 37 meV (ZnTe). Other studies for II-VI compounds support this trend [71,72,89]. Our results are in agreement with the usual 2H-3C gap difference in other compounds such as III-V where the ZB-WZ polytypism has been observed [46].

The effective masses of the uppermost three valence bands and the lowest conduction band are given for the 3C polytypes in Table V. The split-off (m_{so}), heavy hole (m_{hh}), light hole (m_{lh}), and the electron (m_e) effective masses were determined numerically by fitting the calculated dispersion curves around the Γ point along the directions [111] (Γ-L) and [100] (Γ-X). For symmetry reasons, the split-off mass and the electron mass are identical along these directions. In general, we found reasonable agreement for the electron, heavy-hole, and light-hole masses. This holds especially for overall values and the chemical trends with anion, they decrease from ZnS over ZnSe to ZnTe. Also relative variations of the light- and heavy-hole masses with the orientation are rather similar. The values in Table V show that the masses of the lh band are by a factor of $m_{hh}/m_{lh} = 3$–15 lighter than the hh ones. There is a clear trend for some underestimation of the band masses within the approximate (QP) theory. The electron masses at the Γ point decrease along the row ZnS, ZnSe, and ZnTe. Note that the conduction band masses in LDA-1/2 are consistently small by about 12%. The largest deviations happen for ZnS.

TABLE VI. Calculated Luttinger parameters for zinc-blende II-VI compounds compared with experimental values in Ref. [92].

Compound	Method	γ_1	γ_2	γ_3
ZnS	LDA-1/2	2.347	0.678	1.050
	Expt.	2.530	0.681	1.050
ZnSe	LDA-1/2	2.539	0.481	1.810
	Expt.	3.350	0.767	1.240
ZnTe	LDA-1/2	4.032	0.996	2.365
	Expt.	3.810	0.838	1.340

TABLE VII. Effective electron and hole masses (in units of free-electron mass m_0) near to Γ of hexagonal (2H) II-VI compounds for different orientations as obtained in LDA-1/2. The results are compared with values from other calculations and experiments.

Compound	Method	$m_e^{\parallel}$	$m_e^{\perp}$	$m_A^{\parallel}$	$m_A^{\perp}$	$m_B^{\parallel}$	$m_B^{\perp}$	$m_C^{\parallel}$	$m_C^{\perp}$
ZnS	LDA-1/2	0.259	0.227	1.380	0.310	0.682	0.357	0.238	0.700
	LDA+U[a]	0.138	0.157	1.785	2.194	0.621	0.195	0.339	0.303
	LDA[a]	0.144	0.153	1.746	3.838	0.756	0.180	0.183	0.337
	Expt.[b]	0.280		1.400	0.490				
ZnSe	LDA-1/2	0.184	0.159	1.745	0.244	0.238	0.422	0.350	0.475
	LDA+U[a]	0.185	0.149	1.629	0.189	0.137	0.187	–	0.344
	LDA[a]	0.148	0.139	1.404	0.158	0.114	0.124	0.171	0.197
ZnTe	LDA-1/2	0.141	0.128	1.294	0.220	0.158	0.342	0.358	0.214
	LDA+U[a]	0.131	0.184	1.116	0.131	0.128	0.166	–	–
	LDA[a]	0.108	0.128	1.042	0.118	0.070	0.105	0.229	0.237
	Expt.[b]	0.130							

[a]From Ref. [90].
[b]From Ref. [91].

Qualitatively they nearly agree with the experimental values. However, the agreement is worse when comparing to results that take the U corrections into account. The LDA+U and LDA theories severely underestimate the electron masses by 40% and 50% in comparison to measured values. This is traced back to the more accurate band-structure calculations with respect to the gap value and the inclusion of SOC. In addition, we have studied the Luttinger parameters of zinc-blende II-VI compounds in Table VI. The four different hh and lh masses given in Table V contain more information than is included in the Kane model [93] of the three uppermost valence bands. In the Kane model these bands are characterized by three Luttinger parameters γ_1, γ_2, and γ_3 [94,95]. Using the LDA-1/2 values, we determine the Luttinger parameters along the Γ-X and the Γ-L direction using the relations

$$\gamma_1 = \frac{m_0}{4}\left(1/m_{\rm hh}^{[111]} + 1/m_{\rm lh}^{[111]} + 1/m_{\rm hh}^{[100]} + 1/m_{\rm lh}^{[100]}\right),$$
$$\gamma_2 = \frac{m_0}{4}\left(1/m_{\rm lh}^{[100]} - 1/m_{\rm hh}^{[100]}\right),$$
$$\gamma_3 = \frac{m_0}{4}\left(1/m_{\rm lh}^{[111]} - 1/m_{\rm hh}^{[111]}\right). \quad (2)$$

We find an increase of the Luttinger parameters from ZnS via ZnSe to ZnTe. The present results are close to the experiment for ZnS. However, we obtain somewhat larger deviations between experimental and computed values for ZnSe and ZnTe.

In the case of the hexagonal 2H the band anisotropy is influenced by the lower crystal symmetry. The uppermost valence bands are isotropic in the plane perpendicular to the c axis due to the lift of the degeneracy at Γ. Therefore, the curvature of the bands along the Γ-M and the Γ-K directions are nearly the same, whereas they differ from the dispersions along the Γ-A direction. The computation of the band masses along Γ-M is difficult because of the lift of the degeneracy of the band states and the displacement of the minima/maxima of these subbands away from Γ due to SOC, i.e., the Rashba effect [96] and Dresselhaus components [97]. In the explicit calculations of effective masses the k-induced splitting due to the spin-orbit interaction of the bands along the ΓM direction have been omitted. The two bands that are degenerate at Γ have been averaged. As a result the masses along ΓM for bands with strong splittings have to be taken with care.

As can be seen from the masses for the hexagonal polytypes (2H) given in Table VII (corresponding Luttinger parameters are listed in Table VIII). The overall agreement especially for the valence bands as well as the conduction band with experiment for electron masses is much better than in the 3C case. This also holds for the comparison with electron masses obtained from LDA+U for ZnSe and ZnTe.

Our calculations also predict an anisotropy of the electron masses of about 12%, 14%, and 9% for ZnS, ZnSe, and ZnTe, respectively. Note that the electron masses are directly related to Γ_{7c} character of conduction bands for all compounds. The hole masses valence bands in Table VII are larger and highly anisotropic compared with electrons. The hh masses are related to the Γ_{9v} band which mainly consists of atomic p_{xy}-like orbitals are much larger, at least in ΓA direction, hence, are more anisotropic. A similar anisotropy has been reported by Karazhanov *et al.* [90] (see Table VII). Note that no clear trend of the hole masses with the different XC functionals is found.

VI. SUMMARY

In summary, we have presented results of first-principles pseudopotential calculations for the structural, energetic,

TABLE VIII. Calculated Luttinger parameters for hexagonal (2H) II-VI compounds.

Compound	Method	A_1	A_2	A_3	A_4	A_5	A_6	A_7
ZnS	LDA-1/2	−4.202	−1.428	3.477	−1.585	0.212	3.060	0.0
ZnSe	LDA-1/2	−2.857	−2.105	2.284	−1.128	0.864	4.060	0.0
ZnTe	LDA-1/2	−2.793	−4.673	2.021	0.938	0.811	3.722	0.0

and electronic band structure properties of cubic (3C) and hexagonal (2H, 4H, and 6H) polytypes of ZnS, ZnSe, and ZnTe II-VI compounds. For the structural parameters, we found good agreement between the calculated and experimental lattice constants a, while a perfect agreement is found for the ratio c/a for the 2H polytype. The lattice parameter a is found to decrease slightly with increasing hexagonality, while the lattice constant ratio is found to increase weakly with hexagonality. The ANNNI model with up to third-nearest neighbor layer interactions provides a good description of the preference for the 3C polytype and stacking faults in cubic materials. The quasiparticle band structures of ZnS, ZnSe, and ZnTe polytypes have been obtained within the recently developed LDA-1/2 method including spin-orbit interaction. The results show very good agreement with the available experimental data for band gaps, spin-orbit splitting energies, and crystal-field splittings. Furthermore, we found a relative weak (strong) dependence of band gap (crystal-field splitting) with hexagonality, while the spin-orbit splitting is practically not influenced by the polytype.

The comparison with measured effective masses shows good agreement with the computed values. In addition, we demonstrate the importance of the spin-orbit interaction for the dispersion and the splittings of the bands around the BZ center and, hence, explain the chemical trend and the symmetry-induced mass splitting.

[1] K. Hiruma, T. Katsuyama, K. Ogawa, M. Koguchi, H. Kakibayashi, and G. P. Morgan, Appl. Phys. Lett. **59**, 431 (1991).

[2] N. W. Jepps and T. F. Page, Prog. Cryst. Growth Charact. Mater. **7**, 259 (1983).

[3] D. Kriegner, C. Panse, B. Mandl, K. A. Dick, M. Keplinger, J. M. Persson, P. Caroff, D. Ercolani, L. Sorba, F. Bechstedt, J. Stangl, and G. Bauer, Nano Lett. **11**, 1483 (2011).

[4] Z. A. Peng and X. Peng, J. Am. Chem. Soc. **124**, 3343 (2002).

[5] L. b. Manna, D. Milliron, A. Meisel, E. Scher, and A. Alivisatos, Nat. Mater. **2**, 382 (2003).

[6] A. Ohtake, J. Nakamura, M. Terauchi, F. Sato, M. Tanaka, K. Kimura, and T. Yao, Phys. Rev. B **63**, 195325 (2001).

[7] S. Li, Y. Jiang, D. Wu, B. Wang, Y. Zhang, J. Li, X. Liu, H. Zhong, L. Chen, and J. Jie, Appl. Phys. A **102**, 469 (2011).

[8] K.-T. Yong, Y. Sahoo, H. Zeng, M. T. Swihart, J. R. Minter, and P. N. Prasad, Chem. Mater. **19**, 4108 (2007).

[9] E. Janik, P. Duewski, S. Kret, A. Presz, H. Kirmse, W. Neumann, W. Zaleszczyk, L. T. Baczewski, A. Petroutchik, E. Dynowska, J. Sadowski, W. Caliebe, G. Karczewski, and T. Wojtowicz, Nanotechnology **18**, 475606 (2007).

[10] Y. Hao, G. Meng, Z. L. Wang, C. Ye, and L. Zhang, Nano Lett. **6**, 1650 (2006).

[11] M. I. B. Utama, M. de la Mata, C. Magen, J. Arbiol, and Q. Xiong, Adv. Funct. Mater. **23**, 1636 (2013).

[12] C. Panse, D. Kriegner, and F. Bechstedt, Phys. Rev. B **84**, 075217 (2011).

[13] A. Belabbes, C. Panse, J. Furthmüller, and F. Bechstedt, Phys. Rev. B **86**, 075208 (2012).

[14] C.-Y. Yeh, Z. W. Lu, S. Froyen, and A. Zunger, Phys. Rev. B **46**, 10086 (1992).

[15] M. Ferhat and A. Zaoui, Appl. Phys. Lett. **88**, 161902 (2006).

[16] M. Ferhat and A. Zaoui, Phys. Rev. B **73**, 115107 (2006).

[17] N. Saidi-Houat, A. Zaoui, and M. Ferhat, J. Phys.: Condens. Matter **19**, 106221 (2007).

[18] C.-Y. Yeh, S.-H. Wei, and A. Zunger, Phys. Rev. B **50**, 2715 (1994).

[19] J. P. Perdew and Y. Wang, Phys. Rev. B **45**, 13244 (1992).

[20] P. E. Blöchl, Phys. Rev. B **50**, 17953 (1994).

[21] A. Dal Corso, Phys. Rev. B **82**, 075116 (2010).

[22] P. Giannozzi, S. Baroni, N. Bonini, M. Calandra, R. Car, C. Cavazzoni, D. Ceresoli, G. L. Chiarotti, M. Cococcioni, I. Dabo, A. Dal Corso, S. de Gironcoli, S. Fabris, G. Fratesi, R. Gebauer, U. Gerstmann, C. Gougoussis, A. Kokalj, M. Lazzeri, L. Martin-Samos, N. Marzari, F. Mauri, R. Mazzarello, S. Paolini, A. Pasquarello, L. Paulatto, C. Sbraccia, S. Scandolo, G. Sclauzero, A. P. Seitsonen, A. Smogunov, P. Umari, and R. M. Wentzcovitch, J. Phys.: Condens. Matter **21**, 395502 (2009).

[23] H. J. Monkhorst and J. D. Pack, Phys. Rev. B **13**, 5188 (1976).

[24] L. G. Ferreira, M. Marques, and L. K. Teles, Phys. Rev. B **78**, 125116 (2008).

[25] L. G. Ferreira, M. Marques, and L. K. Teles, AIP Adv. **1**, 032119 (2011).

[26] M. S. Hybertsen and S. G. Louie, Phys. Rev. B **37**, 2733 (1988).

[27] W. Kohn and L. J. Sham, Phys. Rev. **140**, A1133 (1965).

[28] F. D. Murnaghan, Proc. Natl. Acad. Sci. U.S.A. **30**, 244 (1944).

[29] A. Belabbes, J. Furthmüller, and F. Bechstedt, Phys. Rev. B **87**, 035305 (2013).

[30] D. Spirkoska, A. L. Efros, W. R. L. Lambrecht, T. Cheiwchanchamnangij, A. Fontcuberta i Morral, and G. Abstreiter, Phys. Rev. B **85**, 045309 (2012).

[31] J. Lähnemann, O. Brandt, U. Jahn, C. Pfüller, C. Roder, P. Dogan, F. Grosse, A. Belabbes, F. Bechstedt, A. Trampert, and L. Geelhaar, Phys. Rev. B **86**, 081302 (2012).

[32] A. Belabbes, L. C. de Carvalho, A. Schleife, and F. Bechstedt, Phys. Rev. B **84**, 125108 (2011).

[33] D. Kriegner, S. Assali, A. Belabbes, T. Etzelstorfer, V. Holý, T. Schülli, F. Bechstedt, E. P. A. M. Bakkers, G. Bauer, and J. Stangl, Phys. Rev. B **88**, 115315 (2013).

[34] R. E. Algra, M. A. Verheijen, M. T. Borgstrom, L.-F. Feiner, G. Immink, W. J. P. van Enckevort, E. Vlieg, and E. P. A. M. Bakkers, Nature (London) **456**, 369 (2008).

[35] P. Caroff, K. Dick, J. Johansson, M. Messing, K. Deppert, and L. Samuelson, Nat. Nano **4**, 50 (2009).

[36] H. Landolt and R. Börnstein, in *Numerical Data and Functional Relationships in Science and Technology*, edited by K.-H. Hellwege, O. Madelung, M. Schulz, and H. Weiss (Springer, Berlin, 1982), Vol. III.

[37] S. Biering and P. Schwerdtfeger, J. Chem. Phys. **136**, 034504 (2012).

[38] O. Madelung, U. Rössler, and M. Schulz, in *II-VI and I-VII Compounds, Semimagnetic Compounds*, edited by L.-B. N. Series (Springer, Berlin, 1999), Vol. III.

[39] B. H. Lee, J. Appl. Phys. **41**, 2988 (1970).

[40] N. Lakshmi, N. M. Rao, R. Venugopal, D. Reddy, and B. Reddy, Mat. Chem. Phys. **82**, 764 (2003).

[41] N. K. Abrikosov, V. B. Bankina, L. V. Porestskaya, L. E. Shelimova, and E. V. Skudnova, *Semiconducting II-VI, IV-IV, and V-IV Compounds* (Plenum, New York, 1969).

[42] O. Madelung and L. Börnstein, (eds.), *Semiconductors, Physics of II-VI and I-VII Compounds, Semimagnetic Semiconductors*, Vol. 17, New Series, Group III, Pt. a (Springer, Berlin, 1982).

[43] A. García and M. L. Cohen, Phys. Rev. B **47**, 4215 (1993).

[44] A. Zaoui, M. Ferhat, B. Khelifa, J. P. Dufour, and H. Aourag, Phys. Status Solidi B **185**, 163 (1994).

[45] E. H. Kisi and M. M. Elcombe, Acta Crystallogr. Sect. C **45**, 1867 (1989).

[46] F. Bechstedt and A. Belabbes, J. Phys.: Condens. Matter **25**, 273201 (2013).

[47] C. Raffy, J. Furthmüller, and F. Bechstedt, Phys. Rev. B **66**, 075201 (2002).

[48] F. Bechstedt, P. Käckell, A. Zywietz, K. Karch, B. Adolph, K. Tenelsen, and J. Furthmüller, Phys. Status Solidi B **202**, 35 (1997).

[49] A.-B. Chen and A. Sher, *Data in Science and Technology; Semiconductors Other Than Group IV Elements and III-V Compounds* (Springer, Berlin, 1992).

[50] R. R. Reeber and G. W. Powell, J. Appl. Phys. **38**, 1531 (1967).

[51] Y. Jiang, X.-M. Meng, J. Liu, Z.-R. Hong, C.-S. Lee, and S.-T. Lee, Adv. Mater. **15**, 1195 (2003).

[52] S. Takeuchi and K. Suzuki, Phys. Status Solidi A **171**, 99 (1999).

[53] J. von Boehm and P. Bak, Phys. Rev. Lett. **42**, 122 (1979).

[54] A. Zywietz, K. Karch, and F. Bechstedt, Phys. Rev. B **54**, 1791 (1996).

[55] P. Käckell, J. Furthmüller, and F. Bechstedt, Phys. Rev. B **60**, 13261 (1999).

[56] P. J. H. Denteneer, in *Atomic Scale Calculations in Materials Science*, edited by J. Tersoff, D. Vanderbilt, and V. Vitek, MRS Symposia Proceedings No. 141 (Materials Research Society, Pittsburgh, 1989).

[57] S. Limpijumnong and W. R. L. Lambrecht, Phys. Rev. B **57**, 12017 (1998).

[58] T. Ito, Jpn. J. Appl. Phys. **37**, L1217 (1998).

[59] H. Zhang, J. Zhang, T. Xu, M. He, and J. Li, RSC Adv. **3**, 3535 (2013).

[60] C. E. E. Volker Heine, C. Cheng, and R. J. Needs, MRS Proc. **242**, 507 (1992).

[61] M. Y. Chou, M. L. Cohen, and S. G. Louie, Phys. Rev. B **32**, 7979 (1985).

[62] A. Gross and H. Teichler, Philos. Mag. Part B **64**, 413 (1991).

[63] P. Käckell, J. Furthmüller, and F. Bechstedt, Phys. Rev. B **58**, 1326 (1998).

[64] S. K. Yadav and R. Ramprasad, Appl. Phys. Lett. **100**, 241903 (2012).

[65] S. O. Kasap and P. Capper, *Springer Handbook of Electronic and Photonic Materials* (Springer, Canada, 2006).

[66] W. H. Strehlow and E. L. Cook, J. Phys. Chem. Ref. Data **2**, 163 (1973).

[67] Edited by O. Madelung, *Semiconductors*, Basic Data, 2nd ed. (Springer, Berlin, 1996).

[68] U. Rossow, T. Werninghaus, D. Zahn, W. Richter, and K. Horn, Thin Solid Films **233**, 176 (1993).

[69] A. D. Milns and D. L. Feucht, *Heterojunctions and Metal-Semiconductors Junctions* (Academic, New York, 1972).

[70] B. Montegu, A. Laugier, and D. Barbier, Phys. Rev. B **19**, 1920 (1979).

[71] O. Zakharov, A. Rubio, X. Blase, M. L. Cohen, and S. G. Louie, Phys. Rev. B **50**, 10780 (1994).

[72] A. Fleszar and W. Hanke, Phys. Rev. B **71**, 045207 (2005).

[73] J. P. Perdew and A. Zunger, Phys. Rev. B **23**, 5048 (1981).

[74] J. P. T. Santos, M. Marques, L. G. Ferreira, R. R. Pelá, and L. K. Teles, Appl. Phys. Lett. **101**, 112403 (2012).

[75] F. Matusalem, M. Ribeiro, Jr., M. Marques, R. R. Pelá, L. G. Ferreira, and L. K. Teles, Phys. Rev. B **88**, 224102 (2013).

[76] A. Belabbes, A. Zaoui, and M. Ferhat, Appl. Phys. Lett. **97**, 242509 (2010).

[77] R. R. Pelá, M. Marques, L. G. Ferreira, J. Furthmüller, and L. K. Teles, Appl. Phys. Lett. **100**, 202408 (2012).

[78] O. P. Silva Filho, M. Ribeiro, R. R. Pelá, L. K. Teles, L. G. Ferreira, and M. Marques, J. Appl. Phys. **114**, 033709 (2013).

[79] M. Ribeiro, L. R. C. Fonseca, T. Sadowski, and R. Ramprasad, J. Appl. Phys. **111**, 073708 (2012).

[80] S. Assali, I. Zardo, S. Plissard, D. Kriegner, M. A. Verheijen, G. Bauer, A. Meijerink, A. Belabbes, F. Bechstedt, J. E. M. Haverkort, and E. P. A. M. Bakkers, Nano Lett. **13**, 1559 (2013).

[81] A. Belabbes, J. Furthmüller, and F. Bechstedt, Phys. Rev. B **84**, 205304 (2011).

[82] W. G. Aulbur, L. Jönsson, and J. W. Wilkins, in *Solid State Physics: Advances in Research and Applications*, edited by H. Ehrenreich and F. Spaepen, Vol. 54 (Academic Press, San Diego, 2000), pp. 1–218.

[83] L. Hedin and S. Lundqvist, in *Advances in Research and Applications*, Solid State Physics, Vol. 23, edited by D. T. Frederick Seiz and H. Ehrenreich (Academic, New York, 1970), pp. 1–181.

[84] M. Shishkin and G. Kresse, Phys. Rev. B **75**, 235102 (2007).

[85] F. Fuchs, J. Furthmüller, F. Bechstedt, M. Shishkin, and G. Kresse, Phys. Rev. B **76**, 115109 (2007).

[86] A. Schleife, F. Fuchs, J. Furthmüller, and F. Bechstedt, Phys. Rev. B **73**, 245212 (2006).

[87] M. Rohlfing, P. Krüger, and J. Pollmann, Phys. Rev. B **57**, 6485 (1998).

[88] S.-H. Wei and A. Zunger, Phys. Rev. B **37**, 8958 (1988).

[89] M. Murayama and T. Nakayama, Phys. Rev. B **49**, 4710 (1994).

[90] S. Z. Karazhanov, P. Ravindran, A. Kjekshus, H. Fjellvg, U. Grossner, and B. G. Svensson, J. Appl. Phys. **100**, 043709 (2006).

[91] Edited by O. Madelung, *Semiconductors: Other than Group IV Elements and III-V Compounds* (Springer, Berlin, 1992).

[92] S. Shokhovets, O. Ambacher, and G. Gobsch, Phys. Rev. B **76**, 125203 (2007).

[93] P. Y. Yu and M. Cardona, *Fundamentals of Semiconductors: Physics and Material Properties* (Springer, Berlin, 1995).

[94] A. V. Rodina and B. K. Meyer, Phys. Rev. B **64**, 245209 (2001).

[95] K. Kim, W. R. L. Lambrecht, B. Segall, and M. van Schilfgaarde, Phys. Rev. B **56**, 7363 (1997).

[96] Y. A. Bychkov and E. I. Rashba, J. Phys. C **17**, 6039 (1984).

[97] G. Dresselhaus, Phys. Rev. **100**, 580 (1955).